MEDSCOPE

MEDSCOPE

MEDiterranean Services Chain based On climate PrEdictions

ERA4CS Joint Call on Researching and Advancing Climate Services Development – Topic B

(GRANT AGREEMENT 689029)

European Climate Observations, Monitoring and Services initiative (2)

Deliverable D2.1

Sources of climate predictability from seasonal to multiannual timescales in the Mediterranean region.

JPI Climate

ERA4CS European Research Area for Climate Services

Deliverable Title	Sources of climate predictability from seasonal to multiannual timescales in the Mediterranean region.
WP number	2
Lead Beneficiary	*Susanna Corti and Ignazio Giuntoli, CNR*
Contributors	*Lauriane Batté, Constantin Ardilouze (CNRM)* *Stefano Materia, Marianna Benassi, Paolo Ruggieri (CMCC)* *Froila Palmeiro, Javier García Serrano (BSC/UB)* *Susanna Corti, Ignazio Giuntoli (CNR)*
Deliverable Due Date	*30/06/2019*
Nature of the Deliverable	R — *R – Report* *SP – Software Package* *D – Dataset* *O - Other*

Version	Date	Modified by	Comments
1	30/06/2019	Susanna Corti	Submitted version with each partners' contribution

Table of contents

EXECUTIVE SUMMARY

This deliverable presents a review of the sources of extended range predictability in the Mediterranean region and summarizes the results of the preliminary analyses performed on the sensitivity experiments described in Milestone M2.1. It is found that the phase of Pacific Decadal Oscillation (PDO) modulates the ENSO teleconnection over the Mediterranean, with an enhanced (damped) response with negative (positive) PDO. A Rossby Wave Ray tracking analysis, carried out to study the impact of sea surface temperatures (SSTs) on waves' propagation shows only partial consistency among models in this respect. The frequency of the two ENSO-sensitive Mediterranean Weather Regimes is modulated by the PDO sign as well, however only one model shows a signal consistent with the reanalysis. The degree to which the models reproduce stratospheric variability was investigated looking at the Sudden Stratospheric Warmings (SSWs). It is found that the idealized experiments ENSO/PDO have a tendency to increase SSW occurrences compared to the control runs, although not significantly. Precipitation anomalies in wet land-initialized and land-prescribed experiments evidence a remote effect of soil moisture on precipitation in the Mediterranean, likely owed to lower-level advection of air moisture resulting from evapotranspiration triggering convective precipitation. Finally, the variability of snow cover – known, in Eurasia, to be linked in late autumn to the following winter Arctic Oscillation – has been investigated considering the atmospheric response to high-low snow cover combined with reduced sea ice in the Barents Sea. Results indicate no clear influence on the stratospheric circulation and suggest that further analyses including additional models are needed to identify robust features of the response to snow cover forcings.

1. Sources of predictability: a review from the literature and the rationale behind the sensitivity experiments (BSC/UB – CNR)

Given the chaotic nature of the climate system, one might question the feasibility of forecasting climate conditions months in advance. Yet, seasonal climate prediction is feasible because atmospheric variability on seasonal time-scales is modulated by slowly-varying boundary conditions, such as sea surface temperature (SST), soil moisture or snow cover extent over northern Asia (see Mariotti et al. 2018 for review), and can retain memory from internal processes with very slow relaxation rates, such as those in the stratosphere (see Tripathi et al. 2015 for review). These fluctuations are not noticeable in day-to-day weather conditions but become evident in seasonal averages, e.g. two/three-month means (e.g. Shukla 1998). Seasonal climate prediction has progressed considerably in the last decades but the tropics remain the region where seasonal forecasts are most successful (see Doblas-Reyes et al. 2013 for review).

In most of the extratropics, and in particular in the North Atlantic-European (NAE) region, the anomalies predicted by general circulation model (GCM)-based seasonal forecast systems have usually been weak and barely added valuable information over a forecast based on climatology or persistence. This can be explained by the high level of atmospheric internal variability, particularly during winter. Half of the winter NAE atmospheric variability is associated with the North Atlantic Oscillation (NAO), a meridional air-mass seesaw tied to the strength of the Azores High and Icelandic Low, which strongly influences European climate on interannual time-scales (see Hurrell et al. 2003 for review). The long-lasting problem in seasonal forecast systems over NAE is thought to be potentially alleviated by better representing stratospheric circulation and stratosphere-troposphere coupling in the models. The surface impact of extratropical stratospheric variability is actually very prominent in the Euro-Atlantic sector, projecting on the NAO pattern. This surface signature holds for both anomalies of the polar stratosphere (e.g. Hitchcock and Simpson 2014; Shaw et al. 2014) and tropical-extratropical stratospheric pathways (e.g. Anstey and Shepherd 2014; Calvo et al. 2018). The stratospheric influence on tropospheric variability has been largely detected and analysed, but not until recently have seasonal forecast systems started to explore the enhanced prediction skill provided by this connection. This potential effect on the forecast quality was long anticipated (e.g. Douville 2009), and the last generation of forecast systems have yielded traces of added skill via the stratosphere (Scaife et al. 2014; Domeisen et al. 2015; Stockdale et al. 2015); however, the precise role of resolving the stratosphere and simulating stratospheric processes is unclear and needs to be properly assessed (Kang et al. 2014; Butler et al. 2016). As reviewed by Kidston et al. (2015), whether seasonal climate predictions can benefit from representing stratosphere-troposphere interactions remains to be tested.

El Niño-Southern Oscillation (ENSO) is the most important source of predictability at seasonal time-scales (e.g. Doblas-Reyes et al. 2013). ENSO can be characterized as a dipole in ocean heat content across the tropical Pacific, in which ocean-atmosphere coupled processes trigger anomalous warm (El Niño) or cold (La Niña) events over the central-eastern equatorial Pacific in conjunction with a zonal pressure seesaw (the Southern Oscillation) between eastern and western regions of the tropical basin (e.g. Chang and Battisti 1998). The ENSO influence on the North Pacific-American (NPA) sector is well known: the atmospheric response displays a wavetrain structure arching northeastward, whose centres of action are organized in the so-called Tropical-Northern Hemisphere (TNH) pattern, which is distinct from the internally-generated Pacific-North America (PNA) pattern (e.g. Robertson and Ghil 1999; Alexander et al. 2002; Straus and Shukla 2002; DeWeaver and Nigam 2002; Nigam 2003; Straus et al. 2007; Bladé et al. 2008). The ENSO influence on the winter NAE atmospheric circulation has only recently been elucidated. The canonical ENSO signal takes place in mid/late-winter, namely January-to-March (JFM), not in the conventional winter season (December-to-February; DJF), and consists of a dipolar surface pressure anomaly that resembles the NAO pattern (e.g. Smith et al. 2012). As reviewed by Brönnimann (2007), this canonical ENSO-NAE teleconnection has been stationary and robust over the past 300 years and is linear for El Niño and La Niña events. The underlying mechanisms of the ENSO-NAE teleconnection however, remain to be properly understood. Tropospheric and stratospheric pathways have been suggested to be at play in settling the canonical response but a unifying framework has been elusive to date.

There are a number of key regions where anomalous soil moisture conditions may quasi-sistematically affect the precipitation variability during the boreal summer. In general these areas are found in dry-wet climate transitional zones, where the coupling between soil moisture and evapotranspiration is strong enough to modulate climate (Koster et al. 2004, Seneviratne et al., 2010). The Mediterranean is one of these regions and indeed few studies assessed the effect of dry soils in amplifying and extend hot temperatures associated with heatwaves in Europe (e.g. Mueller and Seneviratne 2012). This suggests that hot day predictions could be substantially improved in operational forecasts with the aid of soil moisture initialization. Fischer et al. (2007) demonstrate that land-atmosphere interactions slightly elongated the duration of the sub-seasonal heatwave episodes and may account for 50–80% of the number of hot days (daily Tmax > 90th percentile) in JJA 2003. Lorenz et al. (2010) identify that simulations in which soil moisture is fixed to a constant value or prescribed seasonal cycle, even with prescribed constant dry conditions, present a lower intrinsic heat wave persistence (5–10% of the spell lengths) than simulations with interactive soil moisture.

A large number of observational and idealised general circulation studies (e.g. Cohen and Entekhabi, 1999; Gong et al., 2003; Fletcher et al. 2007, Peings et al., 2012, Orsolini et al., 2013, Jeong et al., 2013) support the notion that Siberian snow cover in autumn might influence the boreal winter atmospheric circulation (i.e. the phase of the Arctic Oscillation) in the following winter. This theory has been deeply debated for its appealing possible impact on predictability of the Northern Hemisphere cold season. Following the conceptual mechanism described by Cohen et al. (2007), a positive snow-cover anomaly in October leads to the early appearance of a strong Siberian cold high, to large amplitudes in the Rossby-wave train and to an upward wave activity flux that weakens the stratospheric polar vortex (Polvani and Waugh, 2004). This weakening/warming might persist for several months and propagates downward to the troposphere (Baldwin and Dunkerton, 1999), favouring a negative tropospheric Arctic Oscillation during the following winter months. This remote snow forcing is also expected to favour anomalous climate conditions over the North Atlantic and adjacent European regions (e.g. Goodess and Jones, 2002). However this mechanism is still poorly captured by general circulation models (Hardiman et al., 2008).

In the following sections a review of the preliminary results from the analysis of the sensitivity experiments described in Milestone M2.1 is provided. It is worth to mention that such experiments - AMIP-like simulations with climatological boundary conditions everywhere except for selected regions where idealized anomalies were superimposed to climatology- were designed to isolate the atmospheric response to specific changes in boundary conditions, trying therefore to disentangle signal from noise.

2. Results from the sensitivity experiments: ENSO/PDO (CMCC, BSC/UB, CNR)

In this section a review of the preliminary results from the analysis of the sensitivity experiments described in Milestone M2.1 is provided. It is worth to mention that such experiments - AMIP-like simulations with climatological boundary conditions everywhere except for selected regions where idealized anomalies were superimposed to climatology - were designed to isolate the atmospheric response to specific changes in boundary conditions, trying therefore to disentangle signal from noise.

2.1 ENSO teleconnection over the Euro-Mediterranean region and the role of PDO modulation (CMCC)

We provide a first analysis of the sensitivity experiment exploring the effects of the low frequency North Pacific SST variability (as the one linked to the different phases of the Pacific Decadal Oscillation) on the ENSO teleconnection, with a special focus on the Euro-Mediterranean sector. The underlying hypothesis is that changes in the surface ocean mean state may affect the atmospheric mechanisms spreading ENSO signal from low to mid-high latitudes. This set of sensitivity experiments have been tailored to address this point, introducing all the possible different combinations of idealized ENSO and PDO SST (see Figure 1) in an AMIP-like model setup. For each SST configuration, there are 50 ensemble members lasting one year from June to May. The PDO signal is stationary (*i.e.* kept constant for all the duration of the simulation), while the ENSO SST pattern follows an idealized seasonal cycle peaking in winter. This set of forced ensemble comes with a control run, accounting for climatological SST.
This common setup has been followed by all the partners participating to this experimental effort. In the following, we will show the results from the CMCC model, CNRM-CM6-1 model (Voldoire et al. 2019) and EC-EARTH model, and we will focus on the positive ENSO (*i.e.* El-Niño) teleconnection.
In Figure 2 the DJF circulation pattern is shown for each model response (CMCC, CNRM-CM6-1, and EC-EARTH in the first, second, and third row respectively). Since the goal is to investigate if and how changes in the SST basic state affect the ENSO signal, here the teleconnection pattern is defined as the 50-member ensemble mean difference between the forced simulations (*i.e.* ENSO, ENSO/PDO+, and ENSO/PDO-) and the reference basic state ones (*i.e.* climatological SST/PDO+ SST/PDO- SST respectively). This choice should allow to recognize the possible modulating effect of the PDO to the ENSO teleconnection, without taking into account the direct PDO effect.

If we focus on results with the CMCC and CNRM-CM6-1 models, a consistent picture may be found. For both models, there is some evidence of a dampened ENSO response in the positive PDO case, and of an amplification of the ENSO teleconnection in the negative PDO case. This behaviour is consistent both in the North Pacific sector, with a weakening/strengthening of the Aleutian low, and in the North Atlantic one, with a damped/reinforced sea level pressure dipole.

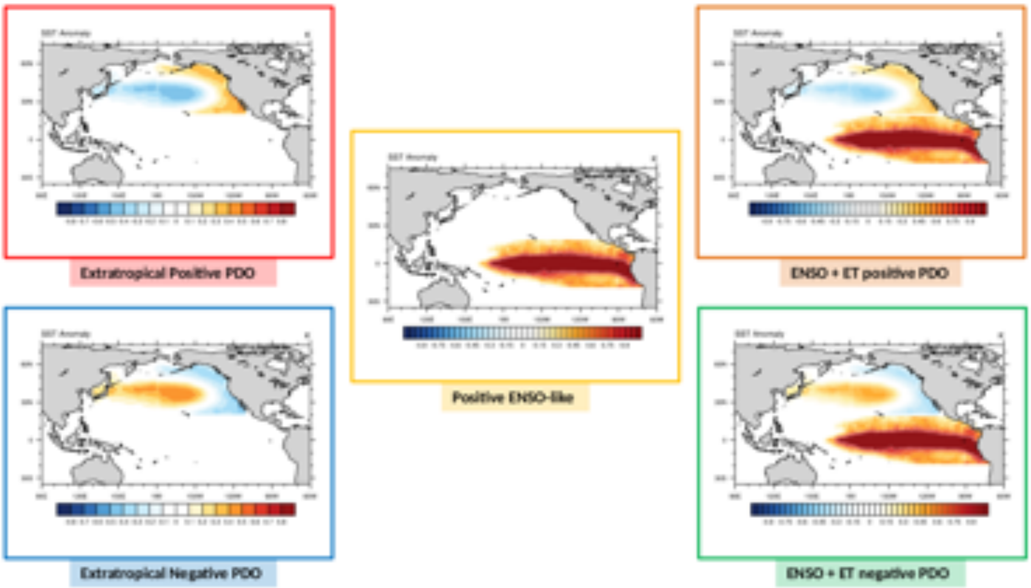

Figure 1: *From left to right: positive and negative PDO-like SST signal, El Niño-like SST signal, and the superposition of El Niño and positive/negative PDO SST signal. These patterns have been computed from the HadISST reanalysis, following the sensitivity experiment protocol (milestone M2.1). In the simulations, these anomalies have been superimposed to a reference climatological SST annual cycle computed always from HadISST reanalysis over the period 1981-2010.*

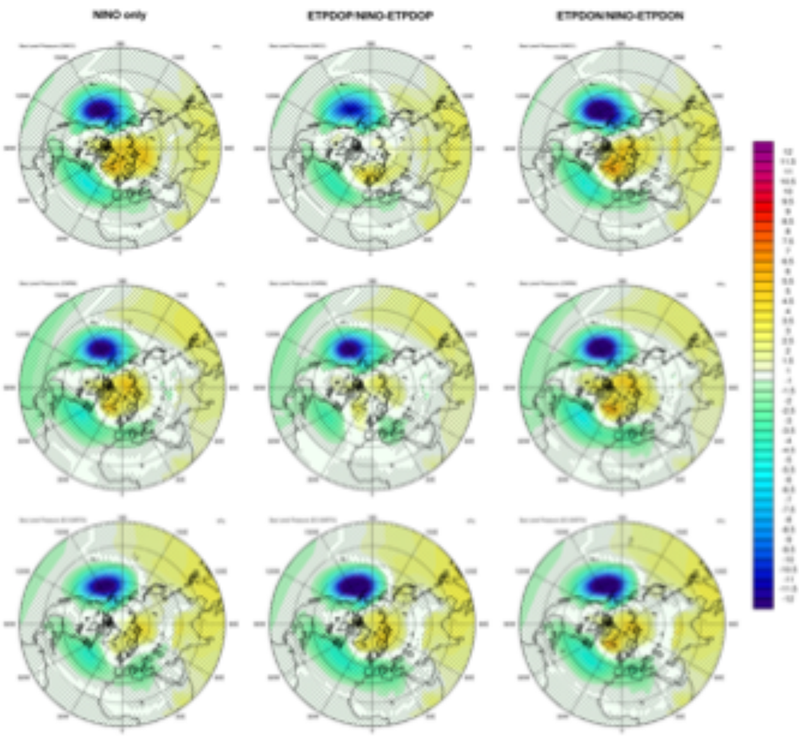

Figure 2: *From top to bottom: CMCC, CNRM-CM6-1 and EC-EARTH DJF sea level pressure teleconnection patterns. In the left column are the reference ENSO signals (ENSO-CTL) for each model, in the central column are the ENSO patterns under positive PDO conditions (ENSO/PDOP – PDOP), and in the right column, are the ENSO patterns under negative PDO conditions (ENSO/PDON – PDON). For each case we take the difference between the 50 member ensemble mean, and the dotted regions are the ones with the 95% confidence level (defined with the t-test)*

EC-EARTH results just partially agree with the picture offered by the other models. In general, both with negative and positive PDO a reinforcement of the ENSO teleconnection is found, which, at least on the North Atlantic, is stronger for the negative PDO case than for the positive PDO one. These results may be summarized by looking at Figure 3 where we show the non-linear component of the response, defined as the residual between the response when the ENSO and PDO SST are included simultaneously in the simulations and the sum of the responses of the ENSO and the PDO experiments separately. The modulating effect of the positive phase of the PDO is generally stronger than the one due to the negative phase of the PDO, especially for CMCC and CNRM-CM6-1. In the case of EC-Earth, the two signals are comparable both in terms of amplitude and of extension of the regions statistically significant.

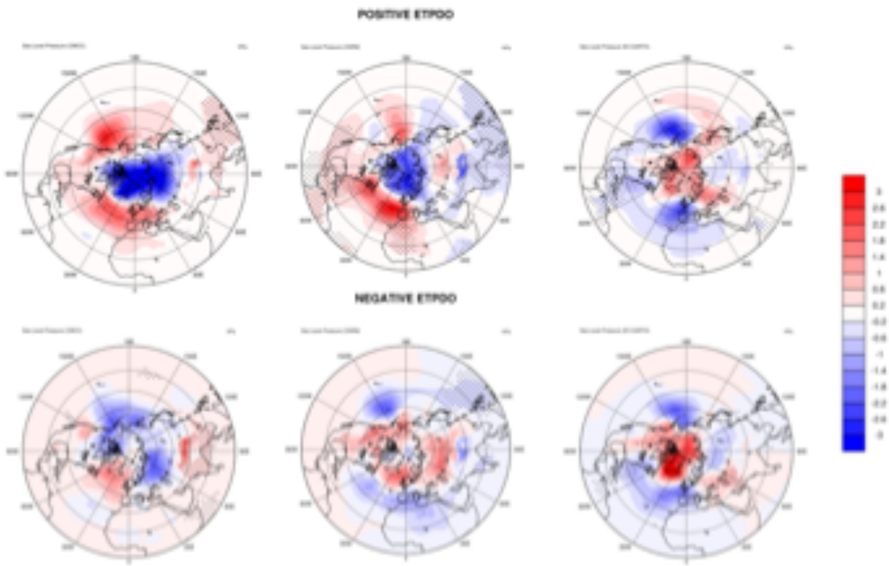

Figure 3: *From left to right: CMCC, CNRM-CM6-1 and EC-EARTH DJF sea level pressure non-linear component of the response defined as ENSO/PDO – (ENSO + PDO). Results for the positive PDO phase are in the top row and the ones for the negative PDO phase are in the bottom row. For each case we take the difference between the 50 member ensemble mean, and the dotted regions are the ones with the 95% confidence level (defined with the t-test).*

The propagation of planetary waves has been suggested as one of the tropospheric mechanisms responsible for the spread of the ENSO signal from low to mid latitudes. We want to explore the impact on the wave propagation of different tropospheric background flows, linked to the different SST conditions we are testing. We propose a Rossby Wave Ray tracing analysis: the ray trajectories are derived integrating the meridional and zonal component of the group velocity equations (as in Karoly, 1983) given the basic state, the initial longitude and latitude of each trajectory, and the initial zonal wavenumber. The basic state zonal and meridional velocity at 200 hPa have to be considered in order to derive all the dynamical quantities needed for the ray tracing integration. For each of the three models, the three different cases (ENSO, ENSO/PDO+, and ENSO/PDO-) are taken into account, and we have defined as basic state the DJF 50-member ensemble average.

Since we are interested in the teleconnection over the Euro-Mediterranean region, in Figure 4 we show the meridional distribution of the trajectories entering in the target domain. To compute these distributions, we have considered the rays with initial zonal wavenumber from 1 to 5 passing through a box from 0E to 5E in longitude, and from 40N to 70N in latitude.

The results from this analysis are not fully conclusive. By comparing CMCC and CNRM-CM6-1 results with EC-EARTH ones, a more spread distribution may be noticed for both ENSO/PDO+ and ENSO/PDO- case for EC-EARTH with respect to CMCC and CNRM-CM6-1, which on the contrary show some agreement of an enhanced maximum over northern latitudes, especially for the ENSO/PDO+ case. However, it should be noted that these results may be affected by the choice of the starting region of the trajectories, and hence by a limited statistic. In this case, all the trajectories are starting from one of the regions of maximum of the Rossby Wave Source field (as defined in Sardeshmukh and Hoskins, 1988) around 28N spanning from 90E to 120E.

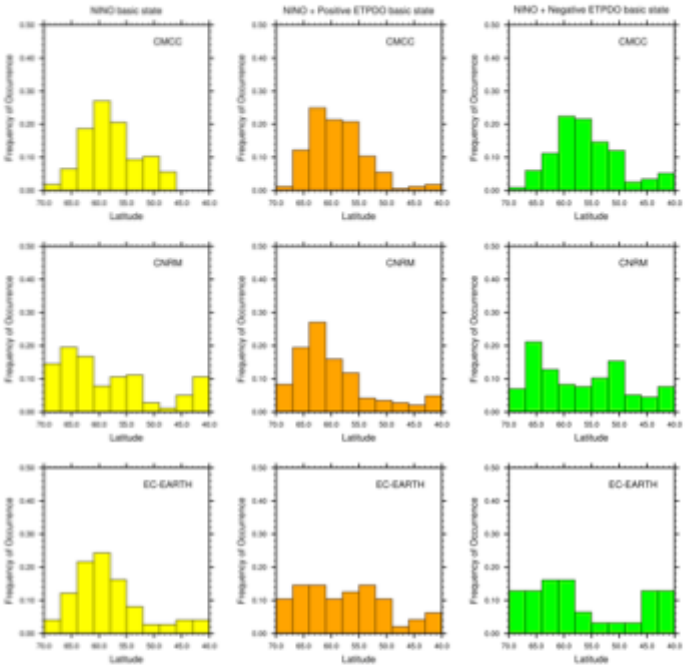

Figure 4: *Meridional distributions of the Rossby Wave ray trajectories entering in the Euro-Mediterranean sector for the ENSO case (left column), and for the ENSO/PDO+ case (central column), for the ENSO/PDO- case (right column). Also in this case, as in Figure 2, results from top to bottom there are for CMCC, CNRM-CM6-1 and EC-EARTH, respectively.*

To have a more definite picture of the impact of the different basic state on the planetary wave propagation a more statistically robust analysis will be performed in the future. Other regions of relative maximum of the Rossby Wave Source field will be explored (*e.g.* the Western Pacific area and the Equatorial Atlantic). Moreover, to increase the number of trajectories, some subsampling of the original 50-member ensemble will be performed: in this way, it will be possible to derive different but statistically and physically equivalent basic state fields for each of the cases considered (ENSO, ENSO/PDO+, and ENSO/PDO-), over which the ray tracing integration will be repeated.

2.2 The role of ENSO in modulating the frequency of Mediterranean Winter Regimes. (CNR)

The ENSO-PDO sensitivity experiments provide a valuable benchmark for assessing how the models respond to specific conditions occurring outside the Mediterranean, namely in the Pacific Ocean. The experiments were set up so that the effect of ENSO and PDO can be studied individually (in their positive/negative mode) or combined. This yields, in addition to a control run (B0), eight different runs: El Niño 1a; El Niño/PDO 1b-c; PDO 2a-b; La Niña 3a; La Niña/PDO 3b-c. In particular, these experiments can be used to assess: (i) the role of ENSO in modulating wintertime Mediterranean Weather Regimes' (MWRs) frequency when opposite phases of the PDO are superimposed and in "unnatural" climatological conditions in different models; (ii) whether the models' MWR response to ENSO is consistent with that found in the reanalysis dataset.

In this preliminary study only CNRM-CM6-1 and EC-Earth experiments have been analyzed. For each model and each experiment DJF MWRs were calculated projecting daily anomalies of 500hPa geopotential height fields on the four leading reanalysis (i.e. ERA-Interim) EOFs (see Deliverable D2.2 for more details on reanalysis EOFs). The cluster centroids obtained from ERA-Interim (D2.2) are then used as reference. The model data is clustered by assigning each model daily anomaly to the nearest ERA-Interim MWR centroid (the patterns of the four DJF MWRs in ERA-Interim are shown in Figure 9 of D2.2). In this way models and reanalysis data share the same phase space and a consistent reanalysis-models MWR picture of the Mediterranean winter variability is obtained. However, it should be noted that the clustering done using each model climatology and computing the clusters using the K-means algorithm as for the reanalysis dataset has shown good agreement in the regime patterns for both CNRM-CM6-1 and EC-Earth models.

Sea surface temperatures (SSTs) composites stratified according to MWR's frequencies in the reanalysis dataset show clear teleconnections with ENSO in two out of four DJF Mediterranean weather regimes, namely DJF MWR1 and MWR3 (termed *meridional* and *anticyclonic*, respectively, as in the study by Rojas et al. 2013). Figures 5 and 6 – bottom panels – depict the global scale SSTs patterns associated to the two regimes, while the three top panels show the weather regimes' centroids as 500 hPa geopotential anomalies (top left), surface air temperature (top middle) and precipitation (top right) over the Mediterranean. MWR1 exhibits a negative temperature anomaly extended over the whole region consistent with increased precipitations over the central-eastern Mediterranean and drier conditions over the Iberian Peninsula. This seasonal anomaly is clearly associated to a La Niña-like pattern. A clear signal pointing to a negative PDO is also evident. On the other hand, MWR3 shows a positive temperature anomaly over central-western Mediterranean, extending and reinforcing in central northern Europe accompanied by drier than normal condition over the Mediterranean. This pattern is related to El Niño-like SSTs anomalies.

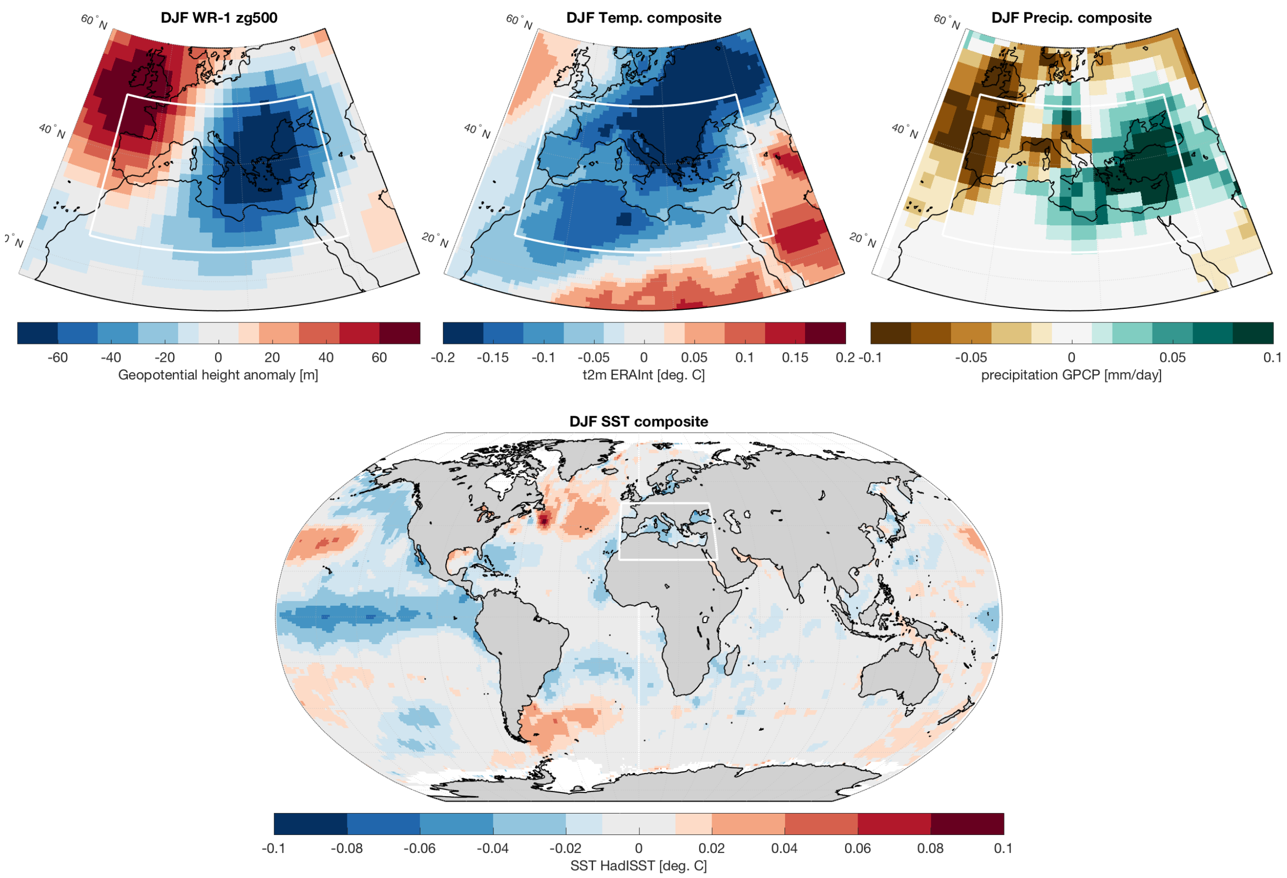

Figure 5: *DJF MWR1 500hPa geopotential height anomaly (top left) and corresponding temperature (top centre) and precipitation patterns (top right). The bottom panel shows the SST composite anomaly stratified according to MWR1 monthly frequency.*

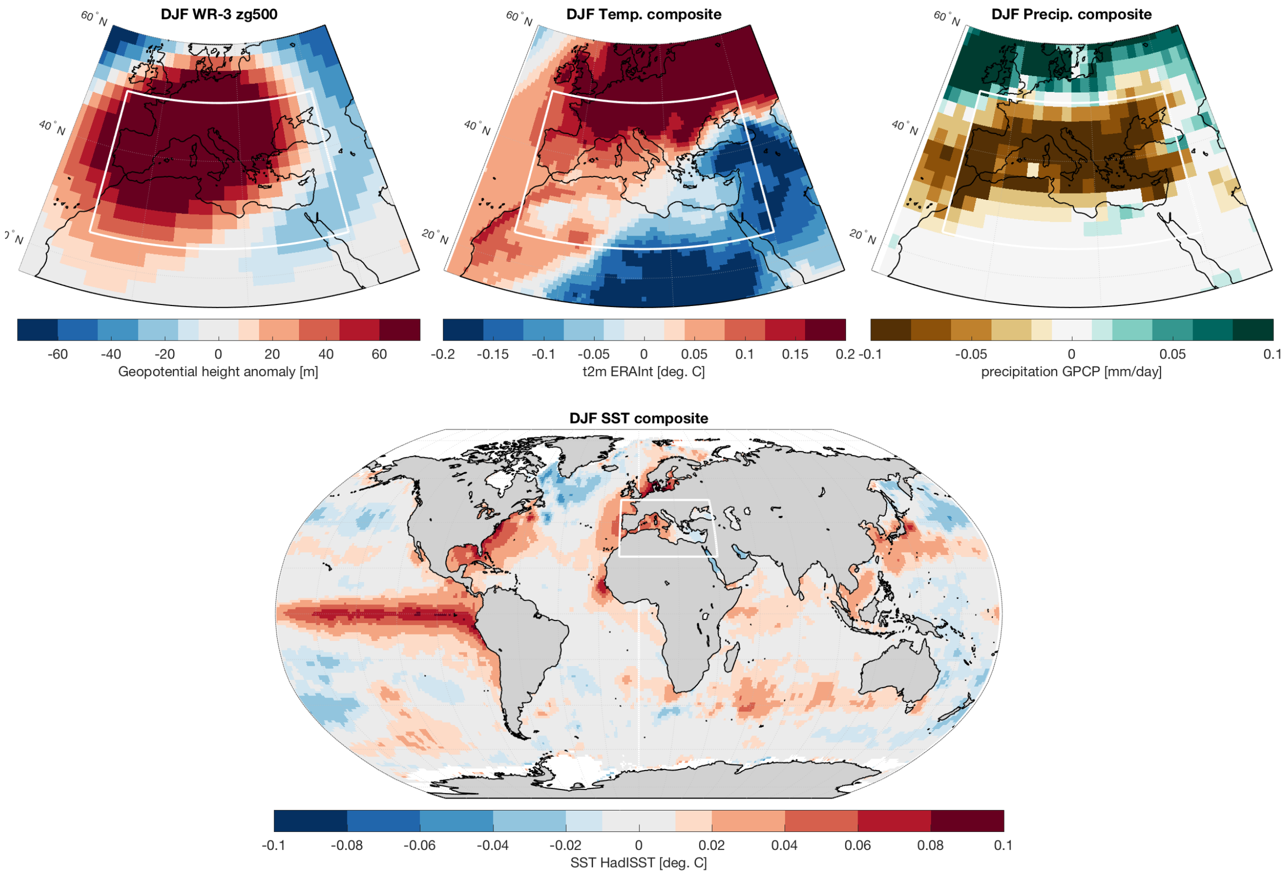

Figure 6: *Same as Figure 5 for WR3.*

The same kind of analysis carried out on the ERA-Interim dataset cannot be applied to the idealized AMIP-like model experiments. However, we can assess if (and how) MWR1 and MWR3 frequencies change in each experiment for the two models considered (i.e. CNRM-CM6-1 and EC-Earth). In particular, we want to verify if: (i) there is a signal of increased MWR1 frequency in the La Niña forced experiments (compared to those forced by El Niño and to the control) and how/if this change is modulated by the PDO sign; (ii) if there is an opposite signal for MWR3 frequencies. Unfortunately, so far, we could verify (i) only with the CNRM-CM6-1 model. The results obtained are summarized in Table 1.

It can be noted that the MWR1 frequency is generally underestimated in both models when compared to ERA-Interim. However, in both models the frequency increases when a PDO anomaly (either negative or positive) is superimposed (compare column B0 with 2a and 2b). In CNRM-CM6-1 MWR1 frequency does increase further when a La-Niña pattern is added to the PDO-. This is indeed very consistent with what we found in the reanalysis, except that in the CNRM-CM6-1 model MWR1 frequency increases too (slightly less though) when the El Niño pattern is added to PDO- (compare 3c and 1c). EC-Earth presents a more complex (and incomplete) picture. MWR1 does increase more with PDO+, and we do not have the combination PDO and La Niña. Therefore a preliminary conclusion is that the SSTs modulation in the Pacific does increase the otherwise underestimated MWR1 frequency in both models, and CNRM-CM6-1 shows the larger sensitivity in the La Niña/PDO- experiment, which is a signal consistent with that found in the reanalysis.

MWR3 frequency is overestimated in B0 by the two models. When the different idealized SSTs forcings are applied, the frequency bias decreases. However, when El Niño and La Niña simulations are compared (with any configuration of the PDO) it seems that, opposite to the reanalysis, in CNRM the regime frequency increases with cold anomalies in the Equatorial Pacific, while EC-Earth does not exhibit an evident “preference ” between El Niño and La Niña.
Overall we can conclude that both models show a sensitivity in the Mediterranean during the boreal winter to ENSO/PDO anomalies and that in general the idealized forcings contribute to decrease the bias in the regimes’ frequencies. However, we found a response consistent with the reanalysis only for MWR1 in the CNRM-CM6-1 experiments.

Table 1 - DJF mean regime frequency for the experiments under CNRM and BSC.

Freq.	ERAInt	B0	1a ElNino	1b ElNino PDO+	1c ElNino PDO-	2a SST PDO+	2b SST PDO-	3a LaNina	3b LaNina PDO+	3c LaNina PDO-
		CNRM-CM6-1								
MWR1	**30.1**	**26.4**	**28.4**	**28.1**	**28.9**	**28.3**	**28.7**	**27.1**	**28.3**	**29.0**
MWR2	26.6	24.7	26.3	25.7	28.1	26.1	26.2	25.6	26.2	26.9
MWR3	**22.0**	**25.0**	**22.5**	**22.9**	**21.6**	**22.8**	**22.8**	**25.5**	**24.0**	**23.7**
MWR4	21.4	24.0	22.8	23.3	21.4	22.8	22.3	21.8	21.6	20.5
		EC-Earth								
MWR1	**30.1**	**27.2**	**27.6**	**28.0**	**28.4**	**28.7**	**28.0**	**27.7**	**-**	**-**
MWR2	26.6	23.9	24.9	23.9	25.2	24.0	24.9	24.8	-	-
MWR3	**22.0**	**25.3**	**24.6**	**24.4**	**23.4**	**24.4**	**23.8**	**24.5**	**-**	**-**
MWR4	21.4	23.6	22.9	23.7	23.1	23.0	23.2	23.1	-	-

2.3 Stratospheric Variability (BSC/UB)

Given the essential role of the stratosphere as a pathway for the tropical to extratropical teleconnections (i.e., the stratospheric pathway), it is important for models to reproduce realistic stratospheric variability and therefore account for the stratosphere-troposphere coupling introduced in Section 1. Sudden Stratospheric Warmings (SSWs) are the main source of variability in the northern winter stratosphere. They consist in the decay of the climatological stratospheric polar vortex with a rapid warming in the middle stratosphere (i.e., tens of degrees in less than a week). The extreme anomalies generated in the stratosphere can propagate downward to the troposphere having a long-lasting impact on the tropospheric circulation that typically projects on a negative NAO (Baldwin and Dunkerton 2001). Therefore, the correct understanding and representation of SSWs in climate models can be used to improve subseasonal and seasonal forecasts, particularly in Europe (e.g., Sigmond et al. 2013, Butler et al. 2019). SSWs are associated to anomalous upward wave propagation from the troposphere to the stratosphere, so certain Pacific SST configurations (e.g., El Niño (EN) or the PDO can favor wave patterns that project onto the climatological ones enhancing wave propagation and thus SSW occurrence. However, the observational records are short and despite the published literature suggests that EN favors SSW occurrence, results are not statistically significant, and the role of the PDO modulating the possible impact of EN cannot be assessed (Song and Son 2018).
In this study, we have detected SSWs as 10 hPa zonal-mean zonal wind reversals at any latitude in the [55 - 70] ºN range from November to March (Palmeiro et al. 2015); this ensures that possible vortex biases in the models are not affecting the SSW counting. Events are separated by at least 21 westerly winds, and final warmings, that occur at the end of every winter, are discarded.
To evaluate the winter stratosphere of the models, we first look at the climatological zonal-mean zonal wind in the middle stratosphere, at 10 hPa and at 65 ºN, close to the edge of stratospheric polar vortex, where easterly winds are expected to be strongest and compare them against Era-Interim (Figure 7a). The three models analised show a seasonal cycle in the polar vortex strength, however, CMCC shows a shift to late winter, and longer lasting persistence of strong values until March, when it starts to decay. CNRM-CM6-1 also shows a stronger polar vortex and a slower weakening than reanalysis. Differently, the seasonal cycle in

EC-EARTH is shifted to early winter and starts to decay in late December. These differences are directly related with the seasonal distribution of SSWs (Figure 7b). For example, SSWs in EC-EARTH show two peaks, in January and February, as in Era-Interim, however, the model shows fewer than normal events in early winter in agreement with the timely stronger polar vortex. The slower decay of the vortex in CNRM-CM6-1 is reflected as an increasing SSW frequency as winter advances, and CMCC shows minimum frequencies in January and February consistent with the plateau of the wind values in Figure 7a. The total decadal frequencies (numbers in the legend) are also in agreement with the polar vortex strength of each model. While EC-EARTH (10.2 SSW/dec) shows the closest SSW frequency to Era-Interim (11.2 SSW/dec), CMCC (9.4SSW/dec) and CNRM-CM6-1 (8.6SSW/dec) show the lowest values having the strongest vortices.

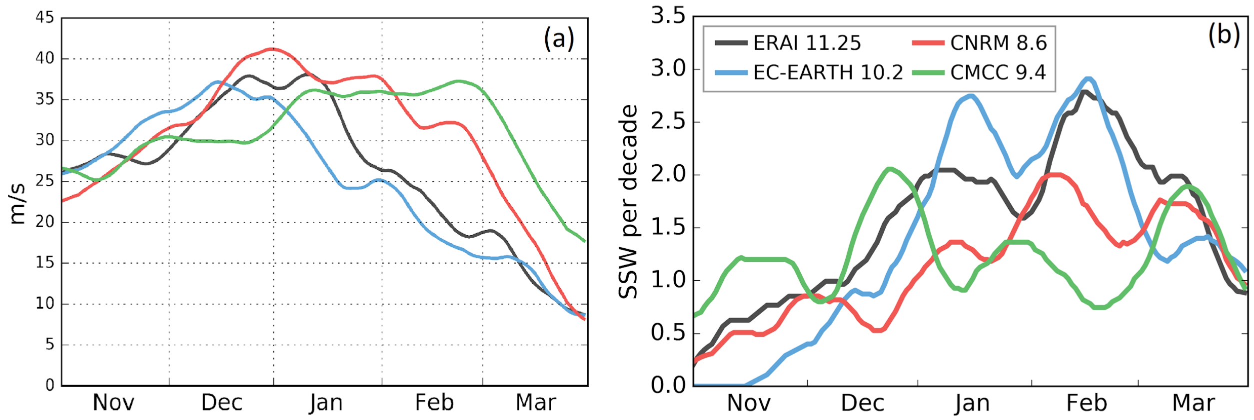

Figure 7: *November to March (a) zonal-mean zonal wind at 65 ºN and 10 hPa and (b) intra-seasonal distribution of SSWs per decade in a [-10, 10]-day window for (blue) EC-EARTH, (red) CNRM-CM6-1, (green) CMCC in the control simulations and (black) ERA-Interim for the 1979-2010 period. Time series are smoothed with a 10-day running mean. Total SSW decadal frequencies are shown in brackets.*

The EN/PDO impact on the total SSW frequency is shown in Figure 8. Models, particularly CMCC, show a tendency of SSWs to occur more frequently during EN than in neutral phases (i.e., CTRL). However, as in the reanalysis, this feature is not statistically significant (Song and Son 2018), so EN alone seems not to be enough to have a clear impact on SSW occurrence. For both phases of the PDO alone, EC-EARTH and CNRM-CM6-1 show more SSWs than in CONTROL, but again, the difference is minimum. On the contrary, in CMCC the PDO reduces the number of SSWs. Although these results are apparently misleading, when looking at the seasonal distribution of SSWs in the PDO experiments, they show an increase in early winter (not shown). Since CMCC already has SSWs in early winter, it is expected that the PDO advancing effect is not reflected. More interestingly, all models agree that EN during both phases of the PDO have an increase of SSWs. This result again reflects the non-linearity of the ENSO/PDO signal that is also effective in the stratosphere. A future analysis at monthly or lower time-scale will help explaining the mechanisms behind these non-linearities and moreover, the differences among models.

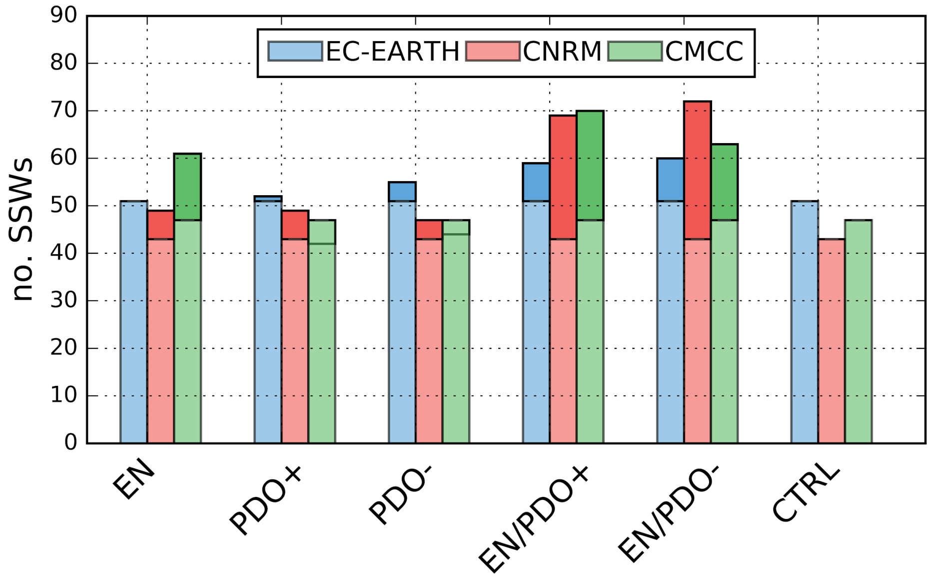

Figure 8: *The total number of SSWs in each experiment for (blue) EC-EARTH, (red) CNRM and (green) CMCC. Light colors show the values for the control simulations and strong colors show the differences EXPERIMENT minus CONTROL. Additional horizontal bars inside the light-colored bars indicate the number of SSWs in the experiment.*

3. Results from the sensitivity experiments: Soil Moisture (CMCC, CNRM)

The land and atmosphere are interlocked by coupled hydrologic and energy cycles that constitute a major part of the Earth's climate system, but the feedback from soil moisture to precipitation via the return path through evapotranspiration (latent heat flux) is weak. Nevertheless, a few studies have addressed the crucial role of soil moisture feedbacks in European droughts, while others assessed the effect of dry soils in amplifying and prolong hot temperatures associated with heat waves in Europe (e.g. Mueller and Seneviratne, 2012). Surface moisture deficits are a relevant factor for the occurrence of hot extremes in many areas of the world, suggesting that the effects of soil moisture-temperature coupling are geographically more widespread than commonly assumed. This implies that hot day predictions could be substantially improved in operational forecasts with the aid of soil moisture initialization. In this work, several sensitivity experiments were performed to assess the role of key climate components on Mediterranean weather at the seasonal time-scale.

Specifically, six experiments have been designed to evaluate the impact of soil moisture on the variability of the summer season over the Mediterranean region. In a region often hit by summer heat waves, the main goal is the assessment of the temperature response to pre-existing a) dry soils, b) wet soils, and c) soils with a "climatological" water content.

To do that, land and atmosphere have alternatively been coupled and uncoupled, and results are shown in Figure 9. An offline run of the land surface model is forced by no precipitation ("dry" experiments **D1** and **D2**, top panels), 3σ precipitation ("wet" experiments **W1** and **W2**, mid panels), climatological precipitation ("climatological" experiments **C1** and **C2**, bottom panels) for one year, until the beginning of the coupled run (May 1st). Left panels show the temperature response of the Mediterranean region for the following May-October semester, when land and atmosphere are coupled to each other; in the right panels, temperature response is shown for the same area, but in this case the soil is maintained, respectively, "dry", "wet", "climatological" for the entire semester.

The strong summer radiation striking dry soils induces higher temperatures and more durable and frequent heat waves in the Mediterranean region, and the effect is more pronounced when atmosphere and land are coupled. If soil is artificially maintained dry for the entire season, temperatures are not allowed to grow as much, except at the end of the hot season, when precipitation should start watering the soil after the end of the dry season. This highlights the crucial role of active air-soil feedbacks on the magnitude of heat waves.
Temperature response to wet initial conditions averagely lasts until mid-summer. When hot air advections hit a wet soil, the moisture mitigating effect is quickly abated, then high temperatures rapidly dry the soil and other heat waves may follow. Instead, if wet conditions are prescribed for the entire season, temperatures remain much lower than heat wave chance is basically canceled.

Results are shown for the CNRM-Cm6-1 model only, similar analysis will be performed shortly with the CMCC-CM model.

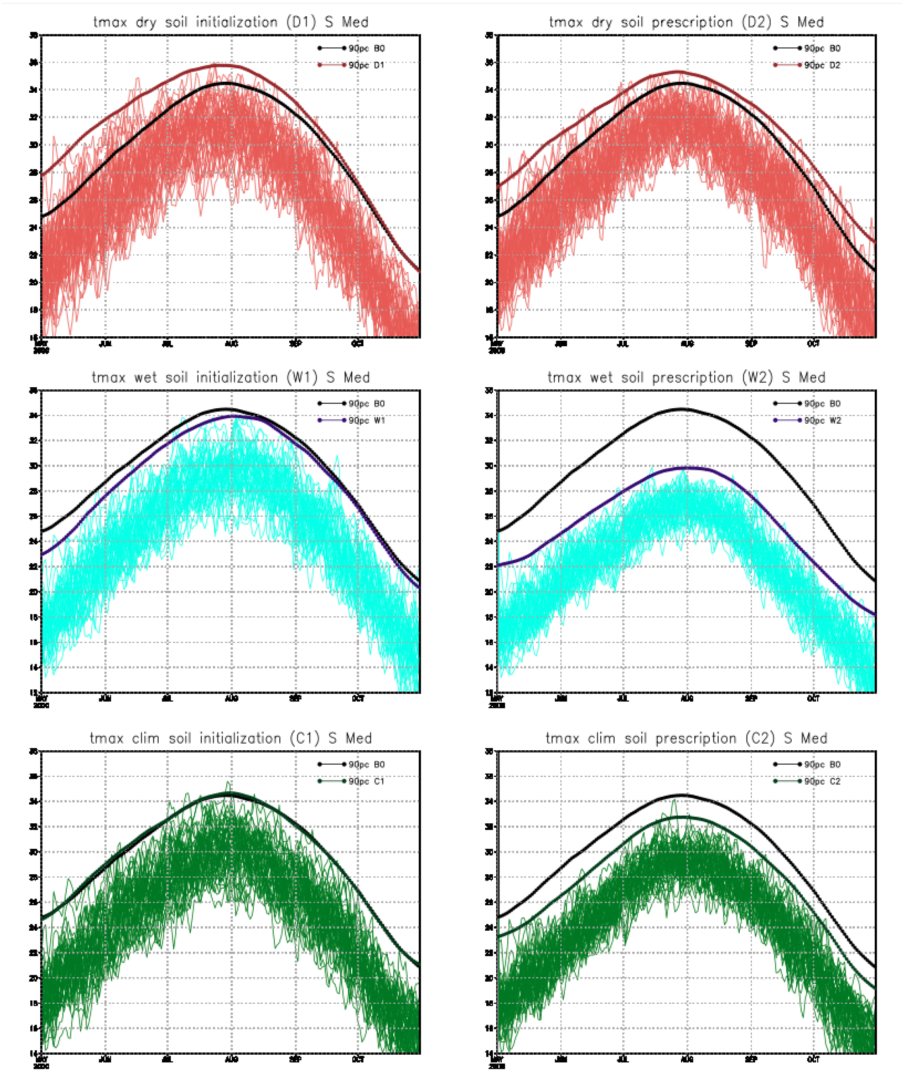

Figure 9: *Daily mean temperature (May 1st Oct 31st) for the (top panels) dry, (center) wet and (bottom) climatological runs. Left panels show the temperature response for the land-initialized experiments, right panels for the land-prescribed experiment. The black (colored) bold line indicates the T2m 90th percentile of the baseline run (sensitivity runs).*

Figure 10 shows the evolution of the average root zone water content over the Mediterranean region during the summer season in the reference run and dry and wet land-initialized and land-prescribed experiments with CNRM-CM6-1 (50 members each). If the dry (D1, D2) and wet (W1, W2) experiments do have the same levels of root zone water content at the initial date, the prescribed experiments maintain, as expected, levels of soil moisture clearly separated from the B0 reference experiments. Note, however, that in the CNRM-

CM6-1 model the effect of an idealized wet or dry initialization is still noticeable 6 months after the start of the simulation.

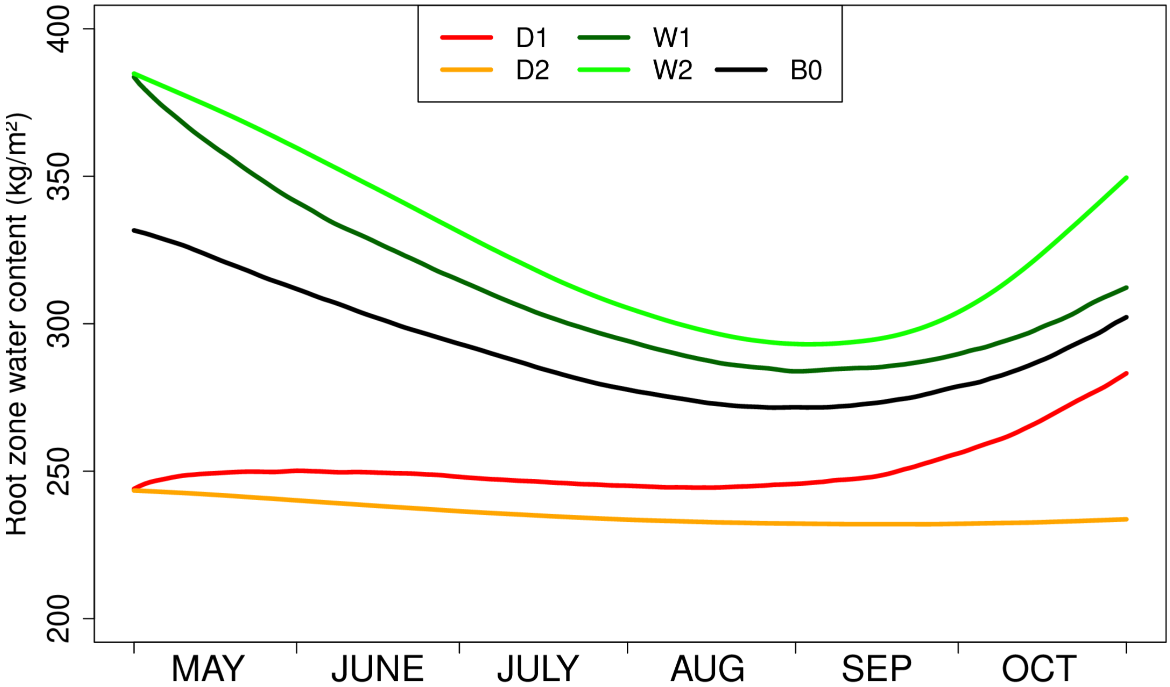

Figure 10: *Evolution of the mean root zone water content over the Mediterranean region in experiments with CNRM-CM6-1: reference (B0, black), land-initialized experiments with dry (D1, red) and wet (W1, dark green) conditions and land-prescribed experiments with dry (D2, orange) and wet (W2, light green) conditions, run from 1st May to 31st October.*

The effect of soil moisture on precipitation in the Mediterranean was also studied, separating the May-October period into three 2-month periods: May-June close to the initialization time of the experiments, July-August corresponding to the peak summer season over the region, and September-October, dynamically more active period when the heavy precipitation events over the Mediterranean start occurring. Figure 11 shows the maps of mean daily precipitation anomalies with respect to the B0 reference experiment in the wet land-initialized (W1) and land-prescribed (W2) experiments. In W2, impacts are (as could be expected) larger than W1 throughout the summer, in particular over the Black and Mediterranean Seas. This suggests a remote effect of soil moisture on precipitation, likely occurring through lower-level advection of air moisture resulting from evapotranspiration which triggers convective precipitation.

To further understand the precipitation anomaly patterns found, we compute the 925 hPa moisture flux anomalies and show the 2-month averages in W2 alongside sea-level pressure anomalies with respect to B0 in Figure 12. High pressure anomalies are found over most of the Mediterranean region, which impacts low-level circulation and therefore advects moist air over the seas of the area, explaining the positive precipitation anomalies found not only over land.

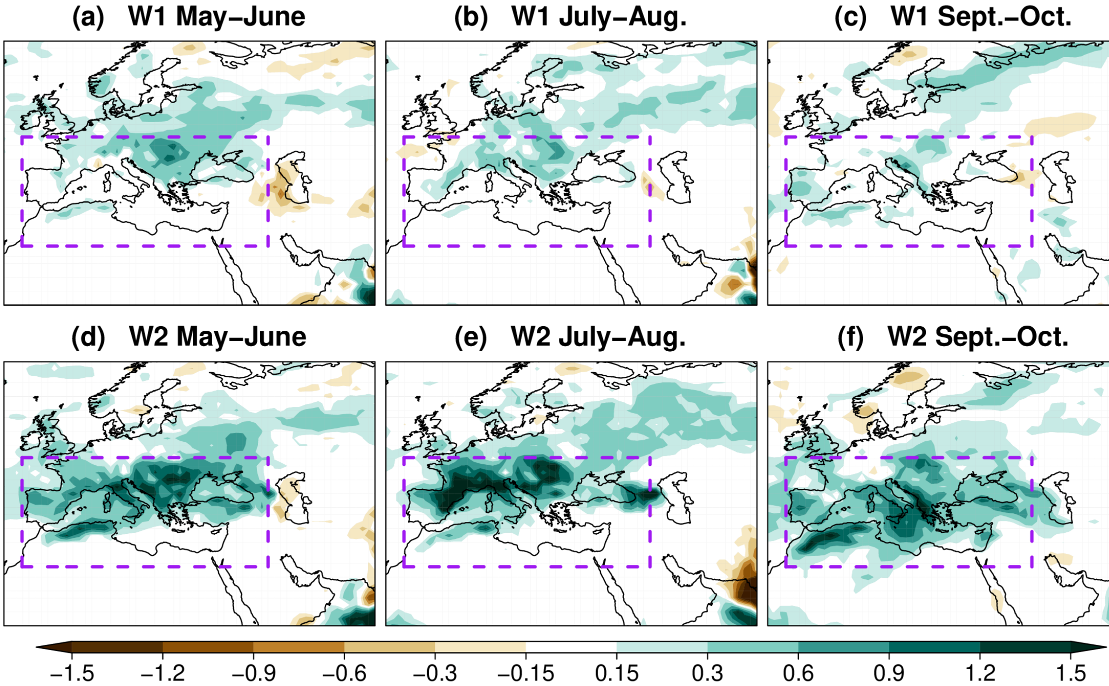

Figure 11: *Impact of wet land initialization (W1) and prescription (W2) on daily mean precipitation (in mm/day) with respect to the B0 reference experiment with CNRM-CM6-1 for May-June (left), July-August (center) and September-October (right). The purple dashed box shows the Mediterranean region.*

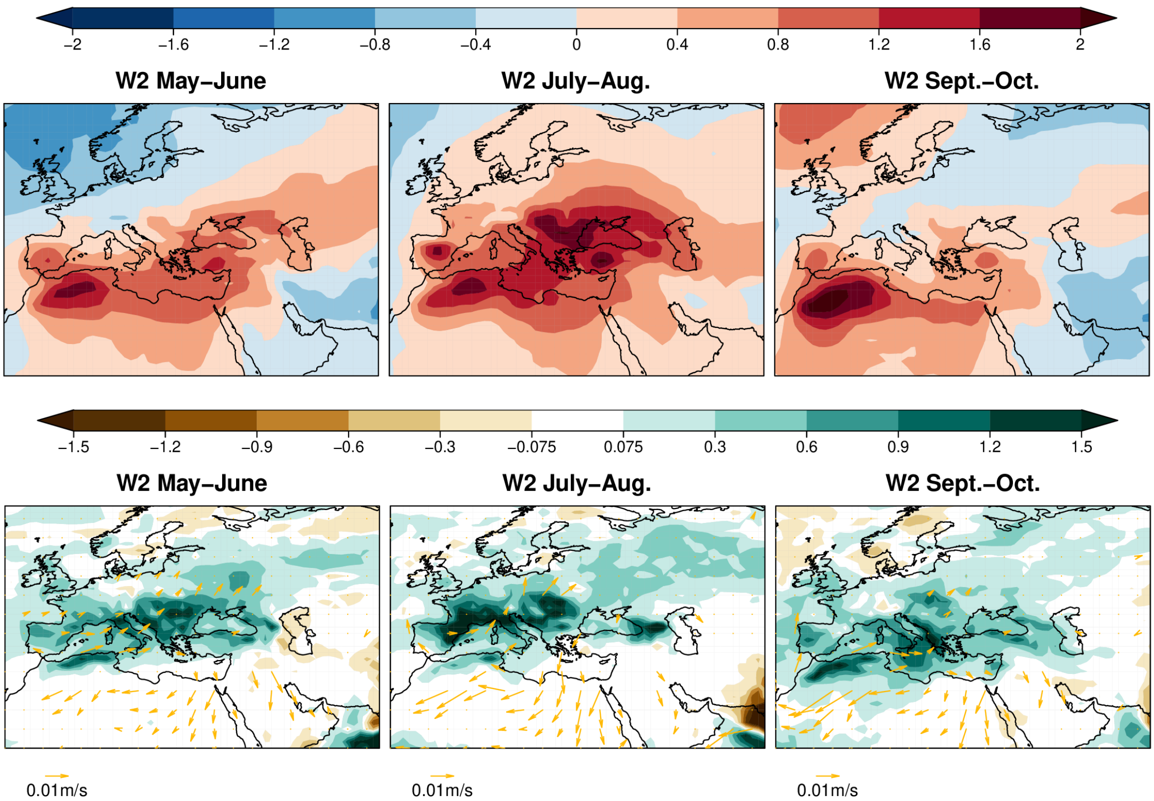

Figure 12: *Mean sea-level pressure anomalies (hPa) (top) and precipitation (mm/day, shading) and moisture flux at 925 hPa anomalies (m/s, arrows) in the wet land-prescribed experiment W2 with respect to baseline experiment B0.*

4. Results from the sensitivity experiments: Snow cover. (CMCC, BSC)

The variability of snow cover in the Eurasian continent in late Autumn has been proposed as a predictor of the subsequent winter Arctic Oscillation, also through a stratospheric pathway (see e.g. Cohen et al 2014a). Hence, there is a potential predictability of the large scale atmospheric flow linked to initialization and prediction of snow cover for winter seasonal forecast initialised in Autumn. Considering the hemispheric scale of the AO, potential impacts would be relevant to many regions of the Northern Hemisphere extratropics. Moreover, a constructive interference between high-snow in Siberia and the recent sea ice loss in the eastern Arctic has been proposed (Cohen et al. 2014b). Nonetheless, the causal role of snow is corroborated by evidence from model experiments and the stationarity of the SNOW/AO relationship has been challenged (Douville et al. 2017). A set of four sensitivity experiments has been designed to investigate the atmospheric response to high-low snow cover combined with reduced sea ice in the Barents sea. In the experiment **SC1a** snow cover in October-November is fixed to the average values observed in November of years with snow cover anomalies above the 75th percentile. In the experiment **SC1b** snow cover October-November average value observed in October of years with snow cover below the 25th percentile. In experiments **SC2a and SC2b** the corresponding snow cover forcing is combined with ice-free conditions in the Barents sea (see Milestone M2.1 for a detailed description of the experimental setup). The baseline for these experiments is **B0**. 50 members initialised on October 1st are run. The ensemble mean response of the near-surface air temperature for the four experiments with the CNRM-CM6-1 model is shown in Figure 13. High snow conditions, revealed by a surface cooling of about 3-4 K, are successfully achieved by the nudging. Instead, in the case of SC1b, low-snow cover conditions are achieved only in a small marginal area of the sector, on the poleward side of the Tibetan Plateau. The reduction of sea ice induces a strong surface warming, larger than 5 K on a wide area in the Barents sea. The dynamical response of the atmosphere to snow cover forcing has been examined in October-November and in December-January, it is generally weak and not significant. No clear evidence of an impact on the stratospheric circulation is found. The geopotential height and sea level pressure response is shown for instance in the left panel of Figure 14. The shallow, statistically significant high over the cooling area is noticeable. Further analysis including other contributing models may be crucial in assessing the robust features of the response to snow cover forcing. The effect of sea-ice reduction can be evaluated comparing SC2a with SC1a or SC2b with SC1b, as done in the middle and right panels of Figure 14. Also in this case the local response over the heating area is baroclinic, with a low below and a high aloft. Two major features are common to both pairs of experiments: the first one is a barotropic high over the eastern Pacific (see also Cvijanovic et al. 2017), while the second one is a weak ridge resembling Ural blocking (see also Ruggieri et al 2017). Unfortunately, the signal is not significant in most areas, and the doubt that the picture may be substantially corrupted by noise is not fully dispelled. Nonetheless, if confirmed by other models, these results can constitute a solid basis for a larger and deeper analysis.

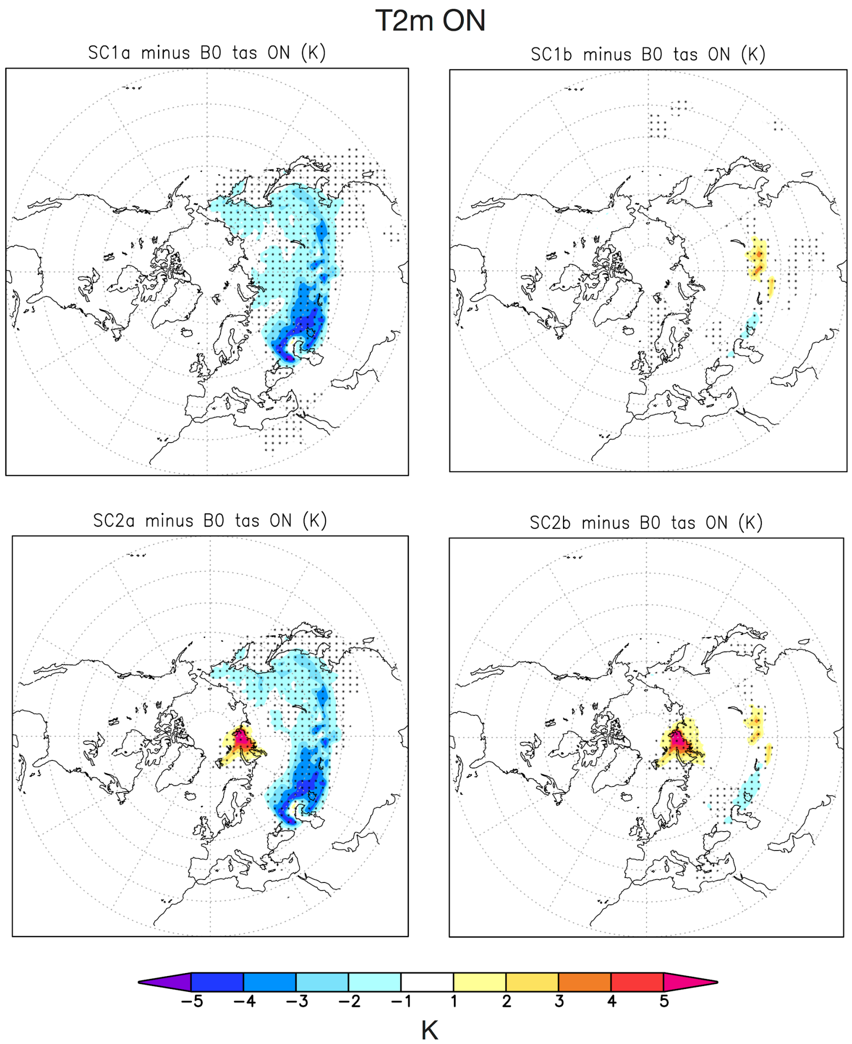

Figure 13: *Difference with respect to B0 of the ensemble mean two-metre temperature (T2m) in October and November for the SC1a (high snow), SC1b (low snow), SC2a (low snow + low ice) and SC2b (low snow + low ice) experiments with the CNRM-CM6-1 model. Stippling indicates statistical significance at the 99% confidence level (t-test).*

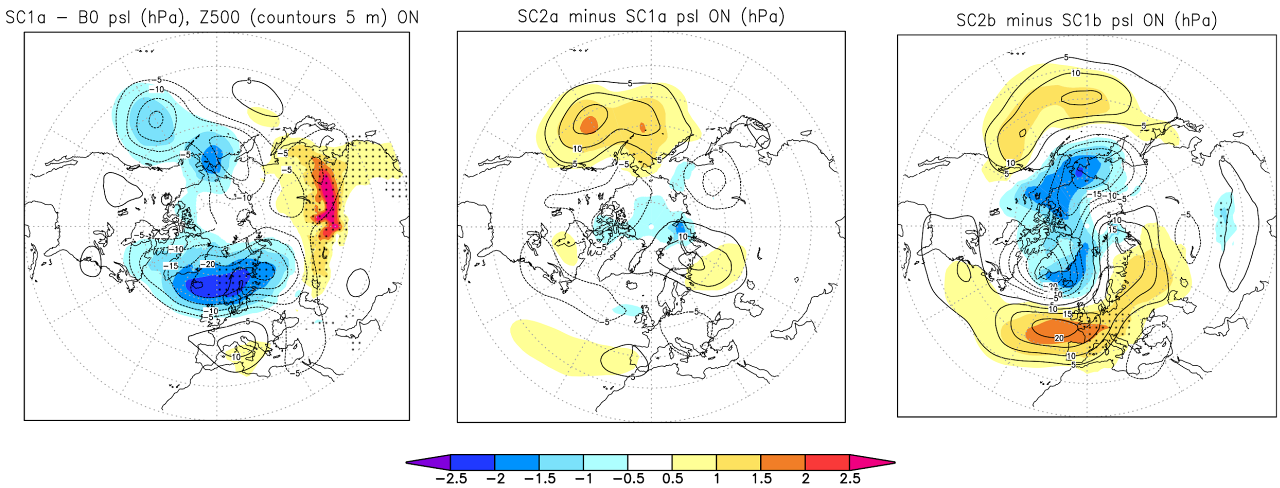

Figure 14: *Sea level pressure (shading) and geopotential height at 500 hPa (contours) difference between SC1a and B0 (left), SC2a and SC1a (middle), SC2b and SC1b (right). Stippling indicates statistical significance (t-test) for the sea level pressure at the 99% confidence level.*

References:

Alexander, M.A., I. Bladé, M. Newman, J.R. Lanzante, N.-C. Lau, J.D. Scott (2002): The atmospheric bridge: the influence of ENSO teleconnections on air-sea interaction over the global oceans. *J. Clim.*, 15, 2205-2231.

Anstey, J.A., T.G. Shepherd (2014): High-latitude influence of the quasi-biennial oscillation. *Q. J. R. Meteorol. Soc.*, 140, doi:10.1002/qj.2132.

Ardilouze, C. (2019b) PhD Manuscript (in French) Impact de l'humidité du sol sur la prévisibilité du climat estival aux moyennes latitudes

Ardilouze, C., Batté, L., Déqué, M., van Meijgaard, E., & van den Hurk, B. (2019a). Investigating the impact of soil moisture on European summer climate in ensemble numerical experiments. *Climate Dynamics*, *52*(7-8), 4011-4026.

Ayarzagüena B., D. Barriopedro, J. M. Garrido-Perez, M. Abalos, A. de la Cámara, R. García-Herrera, N. Calvo and C. Ordóñez. (2018): Stratospheric connection to the abrupt end of the 2016/2017 Iberian drought. *Geophys. Res. Lett.*, 45(22), 12,639-12,646.

Baldwin, M., and T. Dunkerton (2001): Stratospheric harbingers of anomalous weather regimes, *J. Atmos. Sci.*, 294, 581–584.

Baldwin, MP, Dunkerton, TJ. 1999. Propagation of the Arctic Oscillation from the stratosphere to the troposphere. *Journal of Geophysical Research—Atmospheres* **104**(D24): 30937– 30946.

Bladé, I., M. Newman, M.A. Alexander, J.D. Scott (2008): The late fall extratropical response to ENSO: sensitivity to coupling and convection in the tropical West Pacific. *J. Clim.*, 21, 6101–6118.

Brönnimann, S. (2007): The impact of El Niño/Southern Oscillation on European climate. *Rev. Geophys.*, 45, doi:10.1029/2006RG000199.

Butler, A., A. Charlton-Perez, D. I. V. Domeisen, C. Garfinkel, E. P. Gerber, P. Hitchcock, A. Y. Karpechko, A. C. Maycock, M. Sigmond, I. Simpson, and S.-W. Son (2019): Sub- seasonal Predictability and the Stratosphere, in Sub-Seasonal to Seasonal Prediction, pp. 223–241, Elsevier, doi:10.1016/B978-0-12-811714-9.00011-5.

Butler, A.H. et al. (2016): The Climate-system Historical Forecast Project: do stratosphere-resolving models make better seasonal climate predictions in boreal winter?. *Q. J. R. Meteorol. Soc.*, 142, 1413-1427.

Calvo, N., M. Iza, M.M. Hurwitz, E. Manzini, C. Pena-Ortiz, A.H. Butler, C. Cagnazzo, S. Ineson, C.I. Garfinkel 2016: Northern Hemisphere stratospheric pathway of different El Nino flavors in CMIP5 models. *J. Clim.*, 30, 4351-4371.

Ceglar, A., A. Toreti, C. Prodhomme, M. Zampieri, M. Turco, and F. J. Doblas-Reyes, 2018: Land-surface initialisation improves seasonal climate prediction skill for maize yield forecast. Sci. Rep., 8, https://doi.org/10.1038/s41598-018-19586-6.

Chang, P., D.S. Battisti (1998): The Physics of El Niño. Physics World, 8, 41-47.

Charlton, A. J. and Polvani, L.M. (2007) A new look at stratospheric sudden warmings. part I: Climatology and modeling benchmarks. Journal of Climate, 20(3):449–469, 2007.

Cohen [a] , J., J.C. Furtado, J. Jones, M. Barlow, D. Whittleston, and D. Entekhabi, 2014: Linking Siberian snow cover to precursor of stratospheric variability. *J. Climate,* **27**,5422–5432, https://doi.org/10.1175/JCLI-D-13-00779.1

Cohen [b], Judah, et al. 2014. Recent Arctic amplification and extreme mid-latitude weather. *Nature geoscience* 7.9 (2014): 627.

Cohen, J, Barlow, M, Kushner, PJ, Saito, K. 2007. Stratosphere-troposphere coupling and links with Eurasian land surface variability. *Journal of Climate* **20**(21): 5335– 5343.

Cohen, J. and C. Fletcher, 2007: Improved skill of Northern Hemisphere winter surface temperature predictions based on land-atmosphere fall anomalies *J. Climate,* **20**, 4118–4132, https://doi.org/10.1175/JCLI4241.1

Cohen, J., and D. Entekhabi (1999): Eurasian snow cover variability and Northern Hemisphere climate predictability, *Geophys. Res. Le$.*, 26, 345–348, doi:10.1029/1998GL900321.

Cvijanovic, I., Santer, B. D., Bonfils, C., Lucas, D. D., Chiang, J. C., & Zimmerman, S. (2017). Future loss of Arctic sea-ice cover could drive a substantial decrease in California's rainfall. *Nature communications*, *8*(1), 1947.

Dee, D. P. et al. (2011), The ERA-Interim reanalysis: configuration and performance of the data assimilation system. *Q.J.R. Meteorol. Soc.*, 137: 553–597. doi: 10.1002/qj.828

DeWeaver, E., S. Nigam (2002): Linearity in ENSO's atmospheric response. *J. Clim.*, 15, 2446-2461.

Doblas-Reyes, F.J., J. García-Serrano, F. Lienert, A. Pintó Biescas, L.R.L. Rodrigues (2013): Seasonal climate predictability and forecasting: status and prospects. *WIREs Climate Change – Advanced Review*, 4, 245-268.

Domeisen, D.I.V., A.H. Buttler, K. Fröhlich, M. Bittner, W.A. Müller, J. Baehr (2015): Seasonal predictability over Europe arising from El Niño and stratospheric variability in the MPI-ESM seasonal prediction system. *J. Clim.*, 28, 256-271.

Douville, H. (2009): Stratospheric polar vortex influence on Northern Hemisphere winter climate variability. *Geophys. Res. Lett.*, 36, L18703, doi:10.1029/2009GL039334.

Douville, H. et al. (2017): Snow-(N)AO relationship revisited over the whole twenieth century, *Geophys. Res. Le .*, 44, 569–577, doi:10.1002/2016GL071584.

Fischer, E.M. et al. (2007): Soil moisture–atmosphere interac$ons during the 2003 European summer heat wave, *J. Clim.*, 20, 5081–5099. doi:10.1175/jcli4288.1.

Fletcher C G, Kushner P J and Cohen J 2007 Stratospheric control of the extratropical circulation response to surface forcing *Geophys. Res. Lett.* **34** L21802

Gong G, Entekhabi D and Cohen J 2003 Modeled Northern Hemisphere winter climate response to realistic Siberian snow anomalies *J. Clim.* **16** 3917–31

Goodess, CM, Jones, PD. 2002. Links between circulation and changes in the characteristics of Iberian rainfall. *International Journal of Climatology* **22**(13): 1593– 1615.

Hardiman, S. C., P. J. Kushner, and J. Cohen (2008): Investigating the ability of general circula$on models to capture the eMects of Eurasian snow cover on winter climate, *J. Geophys. Res.*, 113, D21123, doi:10.1029/2008JD010623.

Hitchcock, P., I. Simpson (2014): The downward influence of stratospheric sudden warmings. *J. Clim.*, 71, 3856-3876.

Hurrell, J.W., Y. Kushnir, G. Ottersen, M. Visbeck (2003) An overview of the North Atlantic Oscillation. In: The North Atlantic Oscillation - Climatic Significance and Environmental Impact. AGU Geophys Monogr 134:1-36.

Jeong J H, Linderholm H W, Woo S H, Folland C, Kim B M, Kim S J and Chen D 2013 Impacts of snow initialization on subseasonal forecasts of surface air temperature for the cold season *J. Clim.* **26** 1956–72

Kang, D., M.-I. Lee, J. Im, D. Kim, H.-M. Kim, H.-S. Kang, S.D. Schubert, A. Arribas, C. MacLachlan (2014): Prediction of the Arctic Oscillation in boreal winter by dynamical seasonal forecasting systems. *Geophys. Res. Lett.*, 41, 3577-3585.

Karoly, D. J. (1983). Rossby wave propagation in a barotropic atmosphere. *Dynamics of Atmospheres and Oceans*, *7*(2), 111-125.

Kidston, J., A.A. Scaife, S.C. Hardiman, D.M. Mitchell, N. Butchart, M.P. Baldwin, L.J. Gray (2015): Stratospheric influence on tropospheric jet streams, storm tracks and surface weather. *Nature Geosci.*, doi:10.1038/NGEO02424.

Koster, R.D.,P.A. Dirmeyer, Z.C. Guo, G. Bonan, E. Chan, P. Cox, C.T.Gordon, S. Kanae, E.Kowalczyk, D. L awrence, P. Liu, C.H. Lu, S. Malyshev, B. McAvaney, K. Mitchell, D. Mocko, T. Oki, K. Oleson, A. Pitman, Y. C. Sud, C.M. Taylor, D. Verseghy, R. Vasic, Y.K. Xue, T. Yamada *Regions of strong coupling between soil moisture and precipitation* Science, 305 (2004), pp. 1138-1140

Lorenz, R. et al. (2010): Persistence of heat waves and its link to soil moisture memory, *Geophys. Res. Le$.*, 37, L09703.

M Sigmond, JF Scinocca, VV Kharin, and TG Shepherd. Enhanced seasonal following stratospheric sudden warmings. Nature Geoscience, 6(2):98, 2013.

Mariotti, A., P.M. Ruti, M. Rixen (2018): Progress in subseasonal to seasonal prediction through a joint weather and climate community effort. *npj Clim. Atmos. Sci.*, 1, 4.

Mueller, B. and S.I. Seneviratne (2012): Hot days induced by precipita$on de)cits at the global scale, *Proc. Nat. Acad. Sc.*, 109, 12398-12403.

Nigam, S. (2003): Teleconnections. In: Holton JR, Pyle JA, Curry JA (eds) Encyclopedia of atmospheric sciences. Academic Press, Elsevier Science, pp 2243-2269.

Orsolini Y, Senan R, Balsamo G, Doblas-Reyes F, Vitart A, Weisheimer A, Carrasco R and Benestad R 2013 Impact of snow initialization on sub-seasonal forecasts *Clim. Dyn.* **41**1969–82

Palmeiro F. M., Barriopedro, D., García-Herrera, R., and Calvo, N (2015) Comparing sudden stratospheric warming definitions in reanalysis data. Journal of Climate, 28(17):6823–6840, 2015.

Peings Y, Saint-Martin D and Douville H 2012 A numerical sensitivity study of the influence of Siberian snow on the Northern Annular Mode *J. Clim.* **25** 592–607

Polvani, LM, Waugh, DW. 2004. Upward wave activity flux as a precursor to extreme stratospheric events and subsequent anomalous surface weather regimes. *Journal of Climate* **17**(18): 3548– 3554.

Rayner, N.A. et al. (2003): Global analyses of sea surface temperature, sea ice, and night marine air temperature since the late nineteenth century. *J. Geophys. Res.: Atmospheres*, *108*(D14), https://doi.org/10.1029/2002JD002670

Robertson, A.W., M. Ghil (1999): Large-scale weather regimes and local climate over the western United States. *J. Clim.*, 12, 1796-1813.

Robinson, D. A. et al. (2012): NOAA Climate Data Record (CDR) of Northern Hemisphere (NH) Snow Cover Extent (SCE), Version 1.NOAA National Centers for Environmental Information. doi: 10.7289/V5N014G9.

Ruggieri, P., Kucharski, F., Buizza, R., & Ambaum, M. H. P. (2017). The transient atmospheric response to a reduction of sea-ice cover in the Barents and Kara Seas. *Quarterly Journal of the Royal Meteorological Society*, *143*(704), 1632-1640.

Russo, S., and Coauthors, 2014: Magnitude of extreme heat waves in present climate and their projection in a warming world. J. Geophys. Res. Atmos., 119, 12,500-12,512, https://doi.org/10.1002/2014JD022098.

Sánchez García, E., Voces Aboy, J., Rodríguez Camino, E. Verification of six operational seasonal forecast systems over Europe and Northern Africa. Technical note, AEMET, 2018. Available at http://medcof.aemet.es/index.php/models-skill-over-mediterranean

Sardeshmukh, P. D., & Hoskins, B. J. (1988). The generation of global rotational flow by steady idealized tropical divergence. *Journal of the Atmospheric Sciences*, *45*(7), 1228-1251.

Scaife, A.A., Yu. Karpechko, M. P. Baldwin, A. Brookshaw, A. H. Butler, R. Eade, M. Gordon, C. MacLachlan, N. Martin, N. Dunstone, and D. Smith. Seasonal winter forecasts and the stratosphere. Atmospheric Science Letters, 17(1):51–56, 2016.

Scaife, A.A. et al. (2014): Skillful long-range prediction of European and North American winters. *Geophys. Res. Lett.*, 41, doi:10.1002/2014GL059637.

Seneviratne, S. I. *et al.* Investigating soil moisture–climate interactions in a changing climate: a review. *Earth Sci. Rev.* **99**, 99–174 (2010)

Shaw, T.A., J. Perlwitz, O. Weiner (2014): Troposphere-stratosphere coupling: links to North Atlantic weather and climate, including their representation in CMIP5 models. *J. Geophys. Res. - Atmos.*, 119, 5864-5880.

Shukla, J. (1998): Predictability in the midst of chaos: a scientific basis for climate forecasting. *Science*, 282, 728-731.

Sigmond, M., J. F. Scinocca, V. V. Kharin, and T. G. Shepherd, (2013): Enhanced seasonal forecast skill following stratospheric sudden warmings. Nat. Geosci., 6, 98–102.

Smith, D.M., A.A. Scaife, B.P. Kirtman (2012): What is the current state of scientific knowledge with regard to seasonal and decadal forecasting?. *Environ. Res. Lett.*, 7, 015602.

Song, K. and S.W. Son. (2018): Revisiting the ENSO–SSW Relationship. *J. Clim.*, 31, (6), 2133-2143.

Stockdale, T., F. Molteni, L. Ferranti (2015): Atmospheric initial conditions and the predictability of the Arctic Oscillation. *Geophys. Res. Lett.*, 42, doi:10.1002/2014GL062681.

Straus D. M., S. Corti and F. Molteni, 2007: *Circulation Regimes: Chaotic Variability vs. SST-Forced Predictability*. Journal of Climate, **20**, 2251-2272

Straus, D.M., J. Shukla (2002): Does ENSO force the PNA? *J. Clim.*, 15, 2340-2358.

Toniazzo, T., and Scaife, A. A. (2006), The influence of ENSO on winter North Atlantic climate, *Geophys. Res. Lett.*, 33, L24704, doi:10.1029/2006GL027881.Tripathi, O.P. et al. (2015): The predictability of the extratropical stratosphere on monthly time-scales and its impact on the skill of tropospheric forecasts. *Q. J. R. Meterorol. Soc.*, 141, 987-1003.

Voldoire, A., Saint-Martin, D., Sénési, S., Decharme, B., Alias, A., Chevallier, M., et al. (2019). Evaluation of CMIP6 DECK experiments with CNRM-CM6-1. *Journal of Advances in Modeling Earth Systems*, 11. https://doi.org/10.1029/2019MS001683